NeuroImage 124 (2016) 762–769

Contents lists available at ScienceDirect

NeuroImage

journal homepage: www.elsevier.com/locate/ynimg

Simulating disease propagation across white matter connectome reveals anatomical substrate for neuropathology staging in amyotrophic lateral sclerosis

Ruben Schmidt [a], Marcel A. de Reus [b], Lianne H. Scholtens [b], Leonard H. van den Berg [a], Martijn P. van den Heuvel [b,*]

[a] Department of Neurology, Brain Center Rudolf Magnus, University Medical Center Utrecht, Utrecht, Netherlands
[b] Department of Psychiatry, Brain Center Rudolf Magnus, University Medical Center Utrecht, Utrecht, Netherlands

ARTICLE INFO

Article history:
Received 14 January 2015
Accepted 3 April 2015
Available online 11 April 2015

Keywords:
White matter connectivity
Diffusion weighted imaging
Amyotrophic lateral sclerosis
Disease spread
pTDP-43 aggregates

ABSTRACT

Amyotrophic lateral sclerosis (ALS) is a fatal neurodegenerative disease, characterized by progressive loss of motor function. While the pathogenesis of ALS remains largely unknown, recent histological examinations of Brettschneider and colleagues have proposed four time-sequential stages of neuropathology in ALS based on levels of phosphorylated 43 kDa TAR DNA-binding protein (pTDP-43) aggregation. What governs dissemination of these aggregates between segregated regions of the brain is unknown. Here, we cross-reference stages of pTDP-43 pathology with in vivo diffusion weighted imaging data of 215 adult healthy control subjects, and reveal that regions involved in pTDP-43 pathology form a strongly interconnected component of the brain network ($p = 0.04$) likely serving as an anatomical infrastructure facilitating pTDP-43 spread. Furthermore, brain regions of subsequent stages of neuropathology are shown to be more closely interconnected than regions of more distant stages ($p = 0.002$). Computational simulation of disease spread from first-stage motor regions across the connections of the brain network reveals a pattern of pTDP-43 aggregation that reflects the stages of sequential involvement in neuropathology ($p = 0.02$), a pattern in favor of the hypothesis of pTDP-43 pathology to spread across the brain along axonal pathways. Our findings thus provide computational evidence of disease spread in ALS to be directed and constrained by the topology of the anatomical brain network.

Introduction

Investigations of the brain's wiring architecture are a powerful approach in the examination of the pathogenic mechanisms of neurological and neuropsychiatric disorders (Pievani et al., 2014; Rowe, 2010). In amyotrophic lateral sclerosis (ALS) – a devastating, rapidly progressive neurodegenerative motor disorder – anatomical connectivity studies have revealed clear white matter impairments, with tracts directly linking to the motor cortex being the most affected (Douaud et al., 2011; Schmidt et al., 2014; Verstraete et al., 2010, 2013). While these observations of macroscopic disease effects allow for important insights regarding the ultimate consequences on the brain, the underlying pathogenic mechanism of ALS remains largely unknown. Histological examinations have identified phosphorylated 43 kDa TAR DNA-binding protein (pTDP-43) aggregates to form a hallmark of disease pathology in sporadic ALS (Brettschneider et al., 2012, 2014; Neumann et al., 2006), potentially a key factor in the pathogenesis. Recently, Brettschneider and colleagues importantly reported a sequential distribution of pTDP-43 aggregates across multiple, anatomically widespread cortical and subcortical brain areas and defined four sequential stages of neuropathology corresponding to disease burden (Table 1) (Brettschneider et al., 2013). How these pTDP-43 aggregates spread, however, remains elusive.

Mechanisms have been proposed for spread of neuropathology including contiguous models, describing cell-to-cell transfer between neighboring cells, and non-contiguous models describing spread between distant cells either via axonal transport (trans-synaptic) or through blood or cerebrospinal fluid (non-synaptic) (Aguzzi and Rajendran, 2009; Braak et al., 2013; Brundin et al., 2010). In the neurodegenerative diseases of Creutzfeldt–Jacob, Alzheimer, Parkinson and Huntington, aggregates of misfolded proteins have been noted to trigger misfolding of the corresponding healthy protein in newly affected regions (Costanzo and Zurzolo, 2013), thus initiating a feedback loop leading to the accumulation and propagation of pathogenic aggregates in a "prion-like" fashion (Lee et al., 2010). In Alzheimer disease and frontotemporal dementia "prion-like" trans-synaptic transmission of

* Corresponding author at: Heidelberglaan 100, A01.126, 3508 GA Utrecht, Netherlands. Fax: +31 88 75 55443.
E-mail address: m.p.vandenheuvel@umcutrecht.nl (M.P. van den Heuvel).

http://dx.doi.org/10.1016/j.neuroimage.2015.04.005

Table 1
Staging of pTDP-43 implicated regions described by Brettschneider and colleagues and the mapping to the human and macaque brain as subjects for anatomical connectivity investigation.

Stage	Implicated regions	Human brain nodes	Macaque cortical nodes
I	Primary motor cortex	Precentral gyrus	B4, B6
	Supplementary motor area	Superior frontal gyrus	SMA, SEF
	Brainstem motor nuclei	Brain stem	–
	Spinal cord	–	–
II	Middle frontal gyrus	Caudal and rostral middle frontal gyri	FEF, B46, B45, B12
	Brainstem reticular formation	–	–
	Precerebellar nuclei	–	–
	Red nucleus	–	–
III	Gyrus rectus	Medial orbitofrontal gyrus	B14
	Orbital gyrus	Lateral orbitofrontal gyrus	B11, B13
	Postcentral neocortex	Postcentral gyrus	B3a[a], B3b[a]
	Striatum	Caudate, putamen, accumbens area	–
IV	Anteromedial temporal lobe	Entorhinal cortex	ER, B35
	Hippocampal formation	Hippocampus	TH

"–" indicates that the region was not covered by the parcellation scheme.
[a] 3a and 3b (postcentral gyrus) were excluded due to insufficient reports on the presence/absence of corticocortical connections to and from these regions in the macaque.

pathogens along connections of the macroscale brain network formed by white matter pathways has been simulated in a recent study (Raj et al., 2012), showing that patterns of cortical atrophy can be predicted by network diffusion models.

Concerning ALS, in vitro studies have revealed aggregates of pTDP-43 to exhibit "prion-like" behavior (Furukawa et al., 2011) and there is accumulating evidence of active pTDP-43 transport in axons of somatomotor neurons (Fallini et al., 2012). Combining post-mortem observations of Brettschneider and colleagues of pTDP-43 to aggregate in multiple cortical and subcortical regions of the brain (Brettschneider et al., 2013) with recent in vivo connectivity studies showing an expanding network of affected white matter connections with disease progression (Verstraete et al., 2013), has led to the hypothesis of misfolded pTDP-43 to spread along axonal pathways of the brain.

To computationally test this hypothesis, we combined the microscopic histological observation of the four stages of the disease by Brettschneider and colleagues with information on macroscopic wiring of the mammalian brain as derived from ultra-high resolution in vivo diffusion weighted imaging (DWI) data of the Human Connectome Project (Van Essen et al., 2013). Using in silico simulations we show evidence of sequential pTDP-43 spread to be directed by the topological structure of the anatomical white matter pathways of the human macroscale connectome. First, we show a dense level of anatomical connectivity between the regions of the four stages of the disease. Second, we show a natural ordering of anatomical connectivity within this subnetwork, an organization that follows the sequential order of pTDP-43 involvement. And third using computational modeling, we show simulated spread from primary motor regions along the anatomical pathways of the human connectome to significantly overlap with the spread of pTDP-43 aggregates as empirically observed by Brettschneider and colleagues. Mapping regions of the four stages to the macaque cortex – allowing for the inclusion of information on directed anatomical pathways as reconstructed from gold standard tract-tracing data – we verify the natural ordering of anatomical connectivity in the connectome to 'guide' or 'direct' disease spread, giving rise to the empirically observed sequential neuropathological stages. Our results illustrate the value of computational simulations in examining and testing potential disease mechanisms.

Materials and methods

Human connectome reconstruction

The human macroscale connectome – a comprehensive map describing all neural connections between large-scale brain regions – was constructed from diffusion weighted MRI of 215 adult healthy control subjects of the Human Connectome Project (HCP, release Q3) (Van Essen et al., 2013). Tissue segmentation was performed on T1 images (voxel size: 0.7 mm isotropic) using Freesurfer (Fischl et al., 2004), followed by a parcellation of the left hemisphere into 42 distinct brain regions, including 34 cortical regions, 7 subcortical structures and the brain stem (Verstraete et al., 2013). For additional cortex-only analyses, parcellation schemes of respectively 68 and 219 cortical regions- both hemispheres- were used (De Reus and van den Heuvel, 2014). Processing of HCP high-resolution DWI data (1.25 mm isotropic, TR/TE = 5520/89.50 ms, multiple b-values, 270 directions, 18 b0 volumes) (Van Essen et al., 2013) included motion, eddy current and susceptibility distortion corrections (Glasser et al., 2013). Anatomical pathways were reconstructed with generalized q-sampling imaging (GQI) and streamline tractography (De Reus and van den Heuvel, 2014), forming a connectome graph of *edges* (reflecting anatomical pathways) and *nodes* (representing brain regions). Numbers of reconstructed streamlines (NOS) were rescaled to a Gaussian distribution (Honey et al., 2009) and were taken as the connectivity strengths (edge weights) of reconstructed pathways. The group-averaged connectome map used for connectivity analyses contained edges present in at least 60% of the subjects (De Reus and van den Heuvel, 2013).

pTDP-43 stages

Investigating white matter connectivity in relation with pTDP-43 neuropathology, anatomical locations of pTDP-43 aggregation as described by Brettschneider (Brettschneider et al., 2013) were mapped to the Desikan-Killiany brain atlas (Cammoun et al., 2012) consisting of 42 distinct brain regions per hemisphere plus the brain stem as used for connectome reconstruction. Brettschneider and colleagues defined four stages of neuropathology based on sequential pTDP-43 involvement, with stage I referring to the regions implicated in ALS cases with least extensive patterns of pTDP-43 pathology: the precentral gyrus, superiorfrontal gyrus and the brain stem. Cases with higher pathological burden also showed pTDP-43 inclusions in stage II regions including the caudal middle frontal and rostral middle frontal gyri followed by stage III regions: medial and lateral orbitofrontal cortex, postcentral gyrus, caudate nucleus, putamen and nucleus accumbens. In patients with most extensive patterns of neuropathology, inclusions extended to stage IV regions including the entorhinal cortex and the hippocampus (Table 1, Fig. 1a).

Anatomical connectivity of pTDP-43 subnetwork

Strengths of connections between nodes of the pTDP-43 subnetwork were tested against connection strengths of connections linking the pTDP-43 component to the rest of the brain using two sample *t*-tests, to examine whether anatomical connectivity may contribute to confinement of spread within the pTDP-43 subnetwork. In addition, to test the significance of the internal wiring strength of the pTDP-43 subnetwork (i.e. the mean strength of connections between pTDP-43 nodes) in an *absolute* sense, instead of *relative* to connectivity strength with the rest of the brain (see above), a null distribution of internal wiring strengths was computed for 1000 random subnetworks. Each random

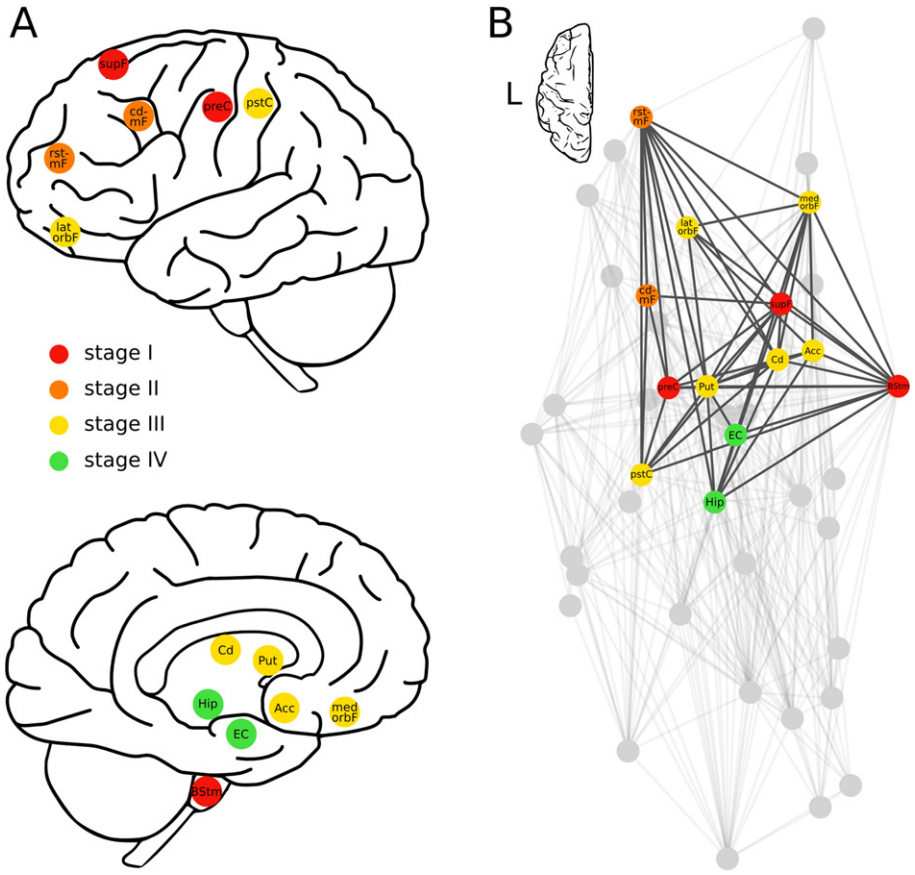

Fig. 1. (A) Brettschneider's regions of stages I (red) to IV (green) of pTDP-43 pathology (see for a description Table 1) which we mapped to the MRI-based parcellation of the brain. (B) Human connectome map (left hemisphere) with nodes involved in pTDP-43 pathology; connections between pTDP-43 regions are highlighted. Nodes are positioned according to the center-of-mass of corresponding brain regions as based on the Freesurfer Desikan-Killiany atlas.

subnetwork was composed of randomly drawn ipsilateral nodes, equal in number to the number of regions in the pTDP-43 subnetwork. The proportion of random subnetworks with an equal or higher internal wiring strength than that of the pTDP-43 subnetwork denoted the p-value.

Sequential ordering in anatomical connectivity

Weighted path length – a graph theoretical metric expressing the minimal sum of inverse weights of connections that need to be traversed when traveling from one node to another in the network – was computed between all nodes, such that shorter weighted paths reflected higher communication efficiency between node pairs (Bullmore and Sporns, 2012; Van den Heuvel and Sporns, 2013). Averaging the weighted path lengths between node pairs of two stages yielded the network topological distance between two stages. A sequential ordering in network topological distances between nodes of stage I, stage I to II, stage I to III and between stage I and IV was evaluated by means of the Jonckheere–Terpstra statistical test, directly testing a staircase ordering effect of successively increasing distances between regions of the four pTDP-43 stages. Similarly, for 1000 random permutations of stage I, II, III and IV labels the Jonckheere–Terpstra test-statistic was evaluated. This way the observed group ordering effect could be compared with a distribution of ordering effects resulting from random configurations of pTDP-43 regions across stages, i.e. the null distribution. The proportion of random permutations showing an equal or stronger increasing group effect among stages yielded the p-value.

In silico simulation of disease spread

Axonal disease spread

A computational random walker spread model (Eubank, 2005; Morelli and Cerdeira, 2004) was used to simulate axonal spread of disease as a walking particle along the pathways of the structural connectome. Starting in one of the stage I regions (i.e. in the precentral gyrus, superior frontal gyrus or in the brain stem, one at a time), a 'random walker' particle was simulated to travel from one brain region to another along network edges (being the anatomical connections). The particle chose an edge from the total set of connections of a node to continue its path (reflecting spread), with the probability of an edge to be chosen proportional to its connectivity strength. When a simulated particle arrived in a brain region (simulating a region becoming affected), in the next step a new random walker emanated from the newly and previously affected regions. Regions were allowed to be revisited, with 2 or more new walkers emanating from a revisited region depending on the number of times it had been visited (simulating aggregation in a positive feedback loop). The process was iterated 5 times, allowing the initial walker to have visited a maximum of 5 other regions besides its seed region (9 iterations for 219 sized cortical parcellations). Repeating this for 10,000 seedings in randomly chosen stage I regions, the amount of aggregated walkers in a region was evaluated as the number of times it had been visited (simulating aggregation of pathology over time). Average levels of total aggregation per stage were tested for an ordering effect using the Jonckheere–Terpstra test. Significance was assessed by comparing the Jonckheere–Terpstra test-statistic against a distribution of values obtained by 1000 random permutations of the stage I, II, III and IV assignments of regions

(referred to as null-model a). Additionally, the significance of stage I regions as potential sources of disease spread was assessed using a null-model choosing random combinations of seed regions 1000, times (null-model b). The proportion of the random permutations yielding a test-statistic larger than that of the actual stage I, II, III and IV regions (null-model a) and with the actual stage I seed regions (null-model b) denoted the p-value.

Spatial disease spread

In simulations of the spatial spread model, in contrast to the axonal model, a 'random walker' particle was simulated to travel from its seed region to any other brain region with the probability of choosing a destination inversely proportional to the Euclidean distance between both regions, preferentially affecting spatially neighboring regions. Upon the walker's arrival the visited region was simulated to become affected too, and a new set of walkers was initiated from the affected regions. Next steps and parameters were identical to the simulations of axonal spread described above.

Validation in the macaque

Analyses and simulations were repeated on a connectome reconstruction of the macaque cortex in order to validate findings on human connectome wiring. Reconstruction of white matter connectivity in the macaque was based on gold standard tract-tracing experiments. Tract-tracing information on anatomical connectivity between 78 non-overlapping regions of the Felleman & Van Essen 91 (FE '91) (Felleman and Van Essen, 1991) anatomical atlas of the macaque cortex was obtained from the freely accessible CoCoMac tract-tracing neuroinformatics database (Stephan et al., 2001). This resulted in a directed 78×78 anatomical connectivity matrix of the macaque cortex (a detailed description of this connectome extraction is provided in Scholtens et al., 2014). pTDP-43 regions of the four stages were mapped to homologous regions in the FE '91 atlas of the macaque cortex (see Table 1).

Results

Anatomical connectivity of pTDP-43 regions

The mapped pTDP-43 regions (Fig. 1b) showed significantly higher mutual connectivity strength (DWI reconstructed fiber streamline count), as compared to connections linking the pTDP-43 regions to the rest of the brain network (11% higher, $p = 1.5 * 10^{-5}$), imposing constraints on spread across axonal pathways from these regions. Furthermore, the average connection strength between regions of the pTDP-43 subnetwork was higher compared to that of random subnetworks ($p = 0.04$), indicating that pTDP-43 affected regions form a strongly anatomically wired subnetwork both in an absolute sense and relative to its embedding in the rest of the brain network.

Sequential ordering in anatomical connectivity

With pTDP-43 regions shown to form a densely interconnected, constrained subnetwork, graph theoretical examination revealed a clear, significant ordering of pTDP-43 regions based on network topological distance. Regions of stages I to IV showed a clear sequential ordering ($p = 0.002$, 1000 random permutations of stage assignments), with network topological distance between regions of stage I being the shortest, followed by the distance between stages I and II, then between I and III, and then between I and IV (Fig. 2a). Network topological distances starting from stage II and III regions showed the same trend of distance increasing with spanned stages (Fig. 2b shows the matrix of network topological distances between all stages). These findings are a first indication of the natural (i.e. healthy) topological structure of brain wiring of the connectome to form an anatomical infrastructure for sequential spread of pTDP-43 pathology between brain regions.

In silico simulation of disease spread

Axonal disease spread

Next, we adopted a computational model to simulate pTDP-43 spread across the connectome. Starting from stage I regions, disease spread was simulated by means of a random walker model, simulating pTDP-43 to travel along connections of the connectome from brain region to region, affecting other regions on its path. This simulation resulted in the highest levels of aggregation to occur in stage I and II regions, followed by stages III and IV, overlapping the exact same sequential stages of neuropathology as empirically observed by Brettschneider (Fig. 3a, $p = 0.02$ compared with random permutations of stage assignments to the pTDP-43 regions (null-model a), $p = 0.015$ compared with random seed regions (null-model b)). Furthermore, simulating aggregation levels across the entire brain network revealed the highest levels of simulated aggregation in regions of the pTDP-43 subnetwork (Fig. 4), with the exception of superior parietal cortex and the thalamus. Aggregation levels in the right hemisphere, contralateral to the seeded regions, showed the same pattern as observed in the left hemisphere, confirming the ordering among pTDP-43 stages.

Cortex-only simulations based on parcellation schemes of, respectively, 68 and 219 regions again yielded a significant ordering effect (68-sized parcellation: $p = 0.05$ (null-model a), $p < 0.001$ (null-model b); 219-sized parcellation: $p = 0.01$ (null-model a), $p = 0.005$ (null-model b)) among simulated aggregation levels overlapping the sequential pTDP-43 involvement (Fig. S1 shows simulated aggregation levels across the cortex using the 68- and 219-sized cortical parcellation schemes).

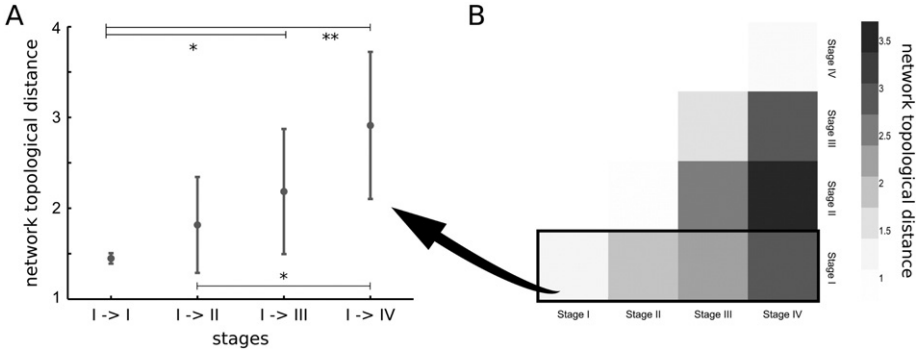

Fig. 2. (A) Network topological distance between nodes of stage I, stage I and stage II, stages I and III and between stages I and IV show a strong ordering effect ($p = 0.002$). Significance of differences in network topological distances between stages is marked as follows: *$p < 0.05$, **$p < 0.005$. (B) Matrix of mean network topological distances between all four stages.

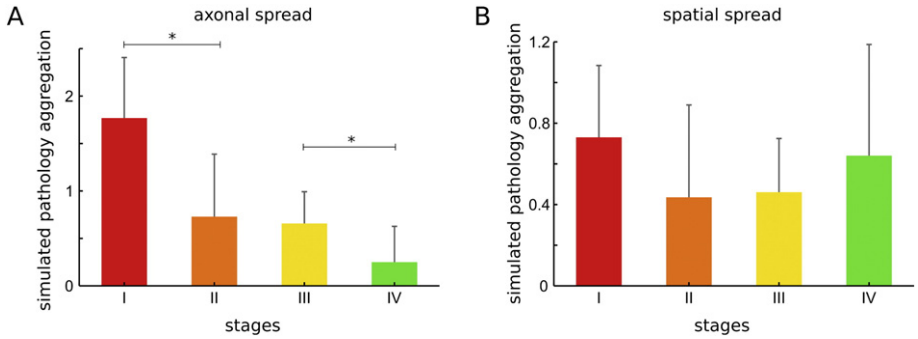

Fig. 3. (A) Simulated axonal spread on the basis of anatomical wiring of the healthy human connectome resulted in highest levels of simulated aggregation in stage I and significantly lower levels in subsequent stages II to IV, an ordering ($p = 0.02$) overlapping the empirical findings of Brettschneider. An asterisk marks the significance of the differences between subsequent stages in simulated aggregation levels: $p < 0.0001$. (B) Modeling spatial spread, no such ordering among stages was observed in the simulated aggregation levels ($p > 0.9$).

Spatial disease spread

A spatial (contiguous) disease spread model – in which spread was dictated by spatial distance from seed regions – was tested against the empirical pTDP-43 staging as an alternative model to axonal disease spread. In contrast to the axonal (non-contiguous) model of disease spread, spatial spread did not result in an ordered pattern of aggregation as observed empirically. Simulations of spatial spread showed no descending pattern (Fig. 3, $p > 0.9$). For the cortical parcellation of 68 regions, levels of simulated pTDP-43 aggregation did show a significant descending pattern over stages (Fig. S1, $p < 10^{-4}$). At the higher resolution cortical parcellation of 219 regions a flat profile of aggregation levels over stages was observed (Fig. S1, $p > 0.9$), a pattern not concurring with the empirical pTDP-43 staging. Simulation findings thus converge on the notion of the anatomical wiring of the brain, rather than spatial distance to underlie sequential pTDP-43 involvement.

Validation in the macaque

A validation analysis on the macaque connectome – with white matter connectivity now defined on the basis of collated tract-tracing data derived from the CoCoMac database – confirmed human DWI findings. First, similar to the human dataset, testing connectivity between homologous pTDP-43 regions in the macaque cortex (Table 1, Fig. 5a) revealed a significantly higher level of connectivity strength between pTDP-43 regions as compared to connections linking the pTDP-43 regions to the rest of the brain ($p = 0.001$). Furthermore, the internal wiring strength of the pTDP-43 subnetwork was found to be significantly stronger than expected based on random subnetworks ($p = 0.007$). Second, again similar to the human data, a significant ordering of increasing network topological distances was present between regions of more distant stages (i.e. I –> I, I –> II, I –> III, I –> IV, $p < 0.001$, 1000 random permutations of stage assignments, Figs. 5b and d). Third, in silico simulations resulted in aggregation levels decreasing with more advanced stages, overlapping the observed pTDP-43 staging (Fig. 5c, $p = 0.02$ compared with random permutations of pTPD-43 regions across stages (null-model a), $p < 0.001$ compared with random seed regions (null-model b)). Taken together, these findings are consistent in all three lines with observations in the human DWI data.

Discussion

Our examination brings forward evidence of pTDP-43 to be propagated along the natural axonal wiring structure of the human brain. Modeling disease spread along the anatomical pathways of the connectome by combining information of recent histology findings of microscale pTDP-43 aggregation in ALS (Brettschneider et al., 2013) with high-resolution DWI of the human brain, reveals three lines of

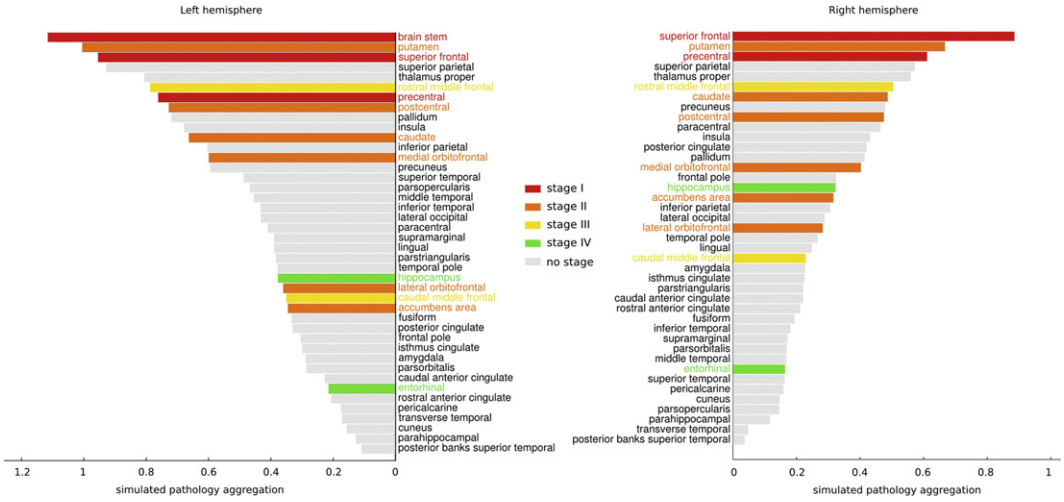

Fig. 4. Simulated levels of pTDP-43 aggregation by the axonal spread model evaluated for all 83 regions of the whole brain parcellation. Aggregation levels in the right hemisphere reflect those in the left hemisphere in which 'random walker' particles were seeded. Stage I and II regions show the highest levels of aggregation in both hemispheres, in accordance with the sequential pTDP-43 involvement.

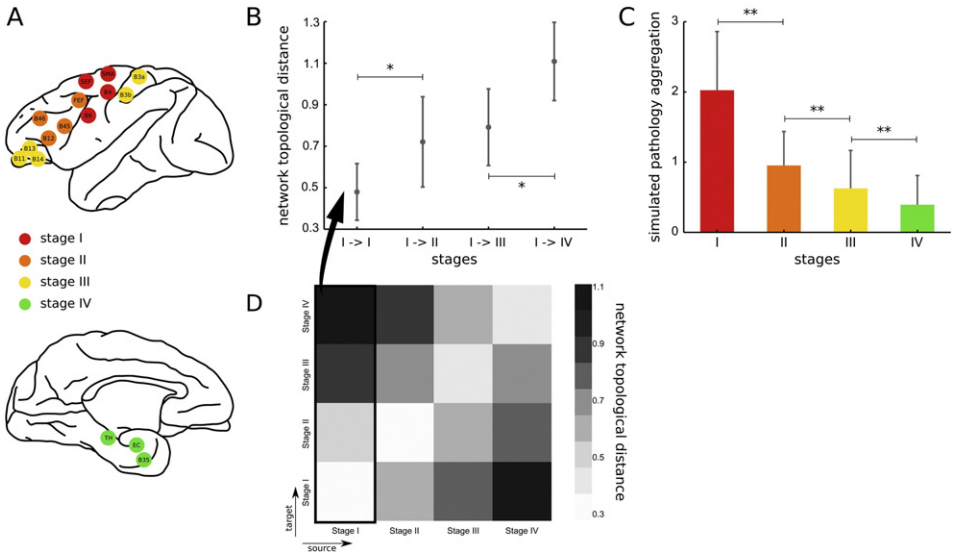

Fig. 5. (A) Schematic representation of homologous regions of neuropathology stages in macaque cortex. (B) Network topological distances between nodes of stage I and more distant stages show a clear ordering effect ($p < 0.001$). Significant differences in network topological distances between stages are marked with an asterisk (*$p < 0.005$). (C) Simulation on the basis of connectome wiring reveals highest aggregation in stage I and significantly lower levels in subsequent stages ($p = 0.009$). Two asterisks mark the significance of the difference between subsequent stages in simulated aggregation levels (**$p < 0.0001$). Results show strong overlap with human findings (Fig. 1). (D) Matrix of network topological distances between all four stages.

evidence that pTDP-43 follows a topological pattern of spread along the anatomical pathways of the brain.

First, examining the level of connectivity between Brettschneider's pTDP-43 regions revealed pTDP-43 implicated regions to form a densely interconnected anatomical subnetwork within the entire brain. The configuration of these regions in a relatively isolated subnetwork underlies the empirical observations of pTDP-43 pathology to initially remain confined to the primary and secondary motor networks. Second, network topological distance between pTDP-43 regions are shown to increase for region pairs spanning more stages, indicative of the underlying white matter wiring architecture of the brain to direct disease spread. A third line of evidence comes from our in silico simulations of axonal disease spread, revealing sequential aggregation from regions in stage I to regions in stage IV, an ordering of regions showing strong overlap with the empirically observed ordering of pTDP-43 involvement in postmortem brains by Brettschneider and colleagues. Moreover, consistent results on all three lines of evidence are observed in macaque data with anatomical connectivity derived from gold standard tract-tracing experiments. Taken together, analyses of the topological organization of the healthy brain's white matter network and simulations of disease spread using a connectome-based model reveal the connectome to intrinsically favor, or guide, the histologically observed sequential staging of neuropathology. Our findings thus suggest the natural topological architecture of the brain's network to form an anatomical infrastructure for disease propagation in ALS.

Comparing simulation results of the axonal and spatial spread models show that sequential pTDP-43 pathology involvement at the macroscale is better explained by our hypothesized non-contiguous, axonal model than by a spatial contiguous mechanism. At the cellular level however, contiguous, cell-to-cell transmission could be at play, supported by patterns of symptom spread to adjacent body regions (Kanouchi et al., 2012) and, more directly, by the detection of Flag TDP-43 messenger RNA contralateral to the injection site in the spinal cord of a primate model (Uchida et al., 2012). Since deceased patients show different burdens of pTDP-43 neuropathology varying from inclusions in stage I regions exclusively to involvement of brain regions of all four stages (Brettschneider et al., 2013), other factors besides propagating pTDP-43 aggregates are likely to contribute to disease progression as well. With recent studies linking macroscale connectome organization to cytoarchitectonic properties of cortical neurons (Beul et al., 2014; Scholtens et al., 2014) future examinations into an interplay between pTDP-43 aggregation at the cellular level and features of macroscopic brain network wiring may provide novel leads towards a better understanding of the pathophysiological mechanisms of ALS.

Brettschneider and colleagues reported the anatomical locations of pTDP-43 aggregates in great detail, specifying subregions within cortical and subcortical structures at a higher spatial resolution than could be provided by the parcellation scheme used for connectome reconstruction. However, apart from these subregions, Brettschneider also noted the spinal cord to form a potentially important stage I region. We were not able to include the spinal cord in our analyses since the field of view of the T1/DWI images contained only the brain. Future studies of in vivo assessments of connectivity in the spinal cord are of high interest. In addition, from stage II, the brainstem reticular formation, precerebellar nuclei and red nucleus could not be one-to-one mapped to the parcellation scheme used for connectome reconstruction, which may have led to an underestimation of simulated aggregation levels in stage II. Furthermore, it should be noted that, despite the expansive histological examinations by Brettschneider and colleagues, for practicability only a limited set of brain regions was assessed for the presence of pTDP-43 inclusions, thereby potentially omitting other implicated regions. No histological information was available on motor associated regions such as the operculum, secondary somatosensory cortex and/or ventral premotor areas and as a result, these regions were not included in our analyses.

While the focus of our paper is on findings in the human that may underlie patterns of pTDP-43 dissemination through the ALS brain, validation of effects in the macaque deserve further consideration. DWI-based connectivity studies have some widely acknowledged limitations, e.g. difficulties in tracing kissing/crossing fibers (Jbabdi and Johansen-berg, 2011; Johansen-Berg and Rushworth, 2009; Pullens et al., 2010) and the possible omission of short, local tracts between adjacent brain regions (Jbabdi and Johansen-berg, 2011). Using human diffusion-derived connectome maps alone, the influence of these methodological issues on our results cannot be gauged. Validation of our findings in the macaque dataset, where connectivity information

is obtained from tract-tracing experiments, suggests that possible artifacts introduced by DWI do not have a great influence on the nature of our findings.

Robustness of our findings against the various parameters used in our analyses and simulations was assessed, reevaluating results for a range of settings. Average connectome maps were obtained using different group thresholds of 50% and 70%, instead of the 60% criterion used in the main analyses, for reevaluation (Supplementary material). Additionally, simulations of pathology aggregation were rerun for a range of steps that the initial walker was allowed to make (2, 4, 6, and 8, see Supplementary material). Above settings of the group threshold revealed consistent results and a walk length of 5 steps was found to be an appropriate setting, see Supplementary material and Fig. S2.

Brettschneider's identification of four distinct stages of neuropathology (Brettschneider et al., 2013) forms an important step towards finding pathogenic mechanisms underlying disease progression in ALS. Their findings have triggered examinations into reduced white matter integrity of pathways specific to these stages in patients (Kassubek et al., 2014). Extending these previous observations, our study now shows evidence of axonal disease spread in agreement with a previous study of our group demonstrating the largest impairments in structural and functional connectivity in connections directly linked to the motor cortex (Schmidt et al., 2014). Findings of disease epicenters in other neurodegenerative disorders, including Alzheimer's disease (Raj et al., 2012; Zhou et al., 2012), suggest a common mechanism of disease propagation for neurodegenerative diseases including ALS.

Conclusions

In this paper we present evidence of the healthy white matter brain network to form an anatomical substrate for the histologically defined neuropathology staging in ALS. Combining histological observations with diffusion weighted imaging data, we show how computational models and simulations may contribute to our comprehension of pathogenic mechanisms.

Disclosure

MPvdH was supported by the Netherlands Organization for Scientific Research VENI Grant, a fellowship of the Brain Center Rudolf Magnus and by the ALS Foundation Netherlands. LHvdB received funding from the Netherlands Organization for Scientific Research VICI Grant and from the ALS Foundation Netherlands. LHvdB received travel grants and consultancy fees from Baxter and serves on scientific advisory boards for Prinses Beatrix Spierfonds, Thierry Latran Foundation, Cytokinetics and Biogen Idec.

Supplementary data to this article can be found online at http://dx.doi.org/10.1016/j.neuroimage.2015.04.005.

Acknowledgments

Data were provided (in part) by the Human Connectome Project, WU-Minn Consortium (Principal Investigators: David Van Essen and Kamil Ugurbil; 1U54MH091657) funded by the 16 NIH Institutes and Centers that support the NIH Blueprint for Neuroscience Research; and by the McDonnell Center for Systems Neuroscience at Washington University.

References

Aguzzi, A., Rajendran, L., 2009. The transcellular spread of cytosolic amyloids, prions, and prionoids. Neuron 64, 783–790. http://dx.doi.org/10.1016/j.neuron.2009.12.016.

Beul, S.F., Grant, S., Hilgetag, C.C., 2014. A predictive model of the cat cortical connectome based on cytoarchitecture and distance. Brain Struct. Funct. http://dx.doi.org/10.1007/s00429-014-0849-y.

Braak, H., Brettschneider, J., Ludolph, A.C., Lee, V.M., Trojanowski, J.Q., Del Tredici, K., 2013. Amyotrophic lateral sclerosis—a model of corticofugal axonal spread. Nat. Rev. Neurol. 9, 708–714. http://dx.doi.org/10.1038/nrneurol.2013.221.

Brettschneider, J., Libon, D.J., Toledo, J.B., Xie, S.X., McCluskey, L., Elman, L., Geser, F., Lee, V.M.Y., Grossman, M., Trojanowski, J.Q., 2012. Microglial activation and TDP-43 pathology correlate with executive dysfunction in amyotrophic lateral sclerosis. Acta Neuropathol. 123, 395–407. http://dx.doi.org/10.1007/s00401-011-0932-x.

Brettschneider, J., Del Tredici, K., Toledo, J.B., Robinson, J.L., Irwin, D.J., Grossman, M., Suh, E., Van Deerlin, V.M., Wood, E.M., Baek, Y., Kwong, L., Lee, E.B., Elman, L., McCluskey, L., Fang, L., Feldengut, S., Ludolph, A.C., Lee, V.M.-Y., Braak, H., Trojanowski, J.Q., 2013. Stages of pTDP-43 pathology in amyotrophic lateral sclerosis. Ann. Neurol. 74, 20–38. http://dx.doi.org/10.1002/ana.23937.

Brettschneider, J., Arai, K., Del Tredici, K., Toledo, J.B., Robinson, J.L., Lee, E.B., Kuwabara, S., Shibuya, K., Irwin, D.J., Fang, L., Van Deerlin, V.M., Elman, L., McCluskey, L., Ludolph, A.C., Lee, V.M.-Y., Braak, H., Trojanowski, J.Q., 2014. TDP-43 pathology and neuronal loss in amyotrophic lateral sclerosis spinal cord. Acta Neuropathol. 423–437. http://dx.doi.org/10.1007/s00401-014-1299-6.

Brundin, P., Melki, R., Kopito, R., 2010. Prion-like Transmission of Protein Aggregates in Neurodegenerative Diseases 11. pp. 301–307.

Bullmore, E., Sporns, O., 2012. The economy of brain network organization. Nat. Rev. Neurosci. 13, 336–349. http://dx.doi.org/10.1038/nrn3214.

Cammoun, L., Gigandet, X., Meskaldji, D., Thiran, J.P., Sporns, O., Do, K.Q., Maeder, P., Meuli, R., Hagmann, P., 2012. Mapping the human connectome at multiple scales with diffusion spectrum MRI. J. Neurosci. Methods 203, 386–397. http://dx.doi.org/10.1016/j.jneumeth.2011.09.031.

Costanzo, M., Zurzolo, C., 2013. The cell biology of prion-like spread of protein aggregates: mechanisms and implication in neurodegeneration. Biochem. J. 452, 1–17. http://dx.doi.org/10.1042/BJ20121898.

De Reus, M.A., van den Heuvel, M.P., 2013. Estimating false positives and negatives in brain networks. NeuroImage 70, 402–409. http://dx.doi.org/10.1016/j.neuroimage.2012.12.066.

De Reus, M.A., van den Heuvel, M.P., 2014. Simulated rich club lesioning in brain networks: a scaffold for communication and integration? Front. Hum. Neurosci. 8, 1–5. http://dx.doi.org/10.3389/fnhum.2014.00647.

Douaud, G., Filippini, N., Knight, S., Talbot, K., Turner, M.R., 2011. Integration of structural and functional magnetic resonance imaging in amyotrophic lateral sclerosis. Brain 134, 3470–3479. http://dx.doi.org/10.1093/brain/awr279.

Eubank, S., 2005. Network based models of infectious disease spread. Jpn. J. Infect. Dis. 58, S9–S13.

Fallini, C., Bassell, G.J., Rossoll, W., 2012. The ALS disease protein TDP-43 is actively transported in motor neuron axons and regulates axon outgrowth. Hum. Mol. Genet. 21, 3703–3718. http://dx.doi.org/10.1093/hmg/dds205.

Felleman, D.J., Van Essen, D.C., 1991. Distributed hierarchical processing in the primate cerebral cortex. Cereb. Cortex 1, 1–47.

Fischl, B., van der Kouwe, A., Destrieux, C., Halgren, E., Ségonne, F., Salat, D.H., Busa, E., Seidman, L.J., Goldstein, J., Kennedy, D., Caviness, V., Makris, N., Rosen, B., Dale, A.M., 2004. Automatically parcellating the human cerebral cortex. Cereb. Cortex 14, 11–22. http://dx.doi.org/10.1093/cercor/bhg087.

Furukawa, Y., Kaneko, K., Watanabe, S., Yamanaka, K., Nukina, N., 2011. A seeding reaction recapitulates intracellular formation of Sarkosyl-insoluble transactivation response element (TAR) DNA-binding protein-43 inclusions. J. Biol. Chem. 286, 18664–18672. http://dx.doi.org/10.1074/jbc.M111.231209.

Glasser, M.F., Sotiropoulos, S.N., Wilson, J.A., Coalson, T.S., Fischl, B., Andersson, J.L., Xu, J., Jbabdi, S., Webster, M., Polimeni, J.R., Van Essen, D.C., Jenkinson, M., 2013. The minimal preprocessing pipelines for the Human Connectome Project. NeuroImage 80, 105–124. http://dx.doi.org/10.1016/j.neuroimage.2013.04.127.

Honey, C.J., Sporns, O., Cammoun, L., Gigandet, X., Thiran, J.P., Meuli, R., Hagmann, P., 2009. Predicting Human Resting-state Functional Connectivity From Structural Connectivity 106. pp. 1–6.

Jbabdi, S., Johansen-berg, H., 2011. Tractography — where do we go from here? Brain Connect. 1, 169–183. http://dx.doi.org/10.1089/brain.2011.0033.Tractography.

Johansen-Berg, H., Rushworth, M.F.S., 2009. Using diffusion imaging to study human connectional anatomy. Annu. Rev. Neurosci. 32, 75–94. http://dx.doi.org/10.1146/annurev.neuro.051508.135735.

Kanouchi, T., Ohkubo, T., Yokota, T., 2012. Can regional spreading of amyotrophic lateral sclerosis motor symptoms be explained by prion-like propagation? J. Neurol. Neurosurg. Psychiatry 83, 739–745. http://dx.doi.org/10.1136/jnnp-2011-301826.

Kassubek, J., Müller, H.-P., Del Tredici, K., Brettschneider, J., Pinkhardt, E.H., Lulé, D., Böhm, S., Braak, H., Ludolph, A.C., 2014. Diffusion tensor imaging analysis of sequential spreading of disease in amyotrophic lateral sclerosis confirms patterns of TDP-43 pathology. Brain 1–8 http://dx.doi.org/10.1093/brain/awu090.

Lee, S.-J., Desplats, P., Sigurdson, C., Tsigelny, I., Masliah, E., 2010. Cell-to-cell transmission of non-prion protein aggregates. Nat. Rev. Neurol. 6, 702–706. http://dx.doi.org/10.1038/nrneurol.2010.145.

Morelli, L., Cerdeira, H., 2004. Aggregation process on complex networks. Phys. Rev. E 69, 051107. http://dx.doi.org/10.1103/PhysRevE.69.051107.

Neumann, M., Sampathu, D.M., Kwong, L.K., Truax, A.C., Micsenyi, M.C., Chou, T.T., Bruce, J., Schuck, T., Grossman, M., Clark, C.M., McCluskey, L.F., Miller, B.L., Masliah, E., Mackenzie, I.R., Feldman, H., Feiden, W., Kretzschmar, H.A., Trojanowski, J.Q., Lee, V.M.-Y., 2006. Ubiquitinated TDP-43 in frontotemporal lobar degeneration and amyotrophic lateral sclerosis. Science 314, 130–133. http://dx.doi.org/10.1126/science.1134108.

Pievani, M., Filippini, N., van den Heuvel, M.P., Cappa, S.F., Frisoni, G.B., 2014. Brain connectivity in neurodegenerative diseases-from phenotype to proteinopathy. Nat. Rev. Neurol. 1–14 http://dx.doi.org/10.1038/nrneurol.2014.178.

Pullens, P., Roebroeck, A., Goebel, R., 2010. Ground truth hardware phantoms for validation of diffusion-weighted MRI applications. J. Magn. Reson. Imaging 32, 482–488. http://dx.doi.org/10.1002/jmri.22243.

Raj, A., Kuceyeski, A., Weiner, M., 2012. A network diffusion model of disease progression in dementia. Neuron 73, 1204–1215. http://dx.doi.org/10.1016/j.neuron.2011.12.040.

Rowe, J.B., 2010. Connectivity analysis is essential to understand neurological disorders. Front. Syst. Neurosci. 4, 1–13. http://dx.doi.org/10.3389/fnsys.2010.00144.

Schmidt, R., Verstraete, E., de Reus, M.A., Veldink, J.H., van den Berg, L.H., van den Heuvel, M.P., 2014. Correlation between structural and functional connectivity impairment in amyotrophic lateral sclerosis. Hum. Brain Mapp. 35, 4386–4395. http://dx.doi.org/10.1002/hbm.22481.

Scholtens, L.H., Schmidt, R., de Reus, M.A., van den Heuvel, M.P., 2014. Linking macroscale graph analytical organization to microscale neuroarchitectonics in the macaque connectome. J. Neurosci. 34, 12192–12205.

Stephan, K.E., Kamper, L., Bozkurt, A., Burns, G.A., Young, M.P., Kötter, R., 2001. Advanced database methodology for the Collation of Connectivity data on the Macaque brain (CoCoMac). Philos. Trans. R. Soc. Lond. B Biol. Sci. 356, 1159–1186. http://dx.doi.org/10.1098/rstb.2001.0908.

Uchida, A., Sasaguri, H., Kimura, N., Tajiri, M., Ohkubo, T., Ono, F., Sakaue, F., Kanai, K., Hirai, T., Sano, T., Shibuya, K., Kobayashi, M., Yamamoto, M., Yokota, S., Kubodera, T., Tomori, M., Sakaki, K., Enomoto, M., Hirai, Y., Kumagai, J., Yasutomi, Y., Mochizuki, H., Kuwabara, S., Uchihara, T., Mizusawa, H., Yokota, T., 2012. Non-human primate model of amyotrophic lateral sclerosis with cytoplasmic mislocalization of TDP-43. Brain 135, 833–846. http://dx.doi.org/10.1093/brain/awr348.

Van den Heuvel, M.P., Sporns, O., 2013. Network hubs in the human brain. Trends Cogn. Sci. 17, 683–696. http://dx.doi.org/10.1016/j.tics.2013.09.012.

Van Essen, D.C., Smith, S.M., Barch, D.M., Behrens, T.E.J., Yacoub, E., Ugurbil, K., 2013. The WU-Minn Human Connectome Project: an overview. NeuroImage 80, 62–79. http://dx.doi.org/10.1016/j.neuroimage.2013.05.041.

Verstraete, E., van den Heuvel, M.P., Veldink, J.H., Blanken, N., Mandl, R.C., Hulshoff Pol, H.E., van den Berg, L.H., 2010. Motor network degeneration in amyotrophic lateral sclerosis: a structural and functional connectivity study. PLoS One 5, e13664. http://dx.doi.org/10.1371/journal.pone.0013664.

Verstraete, E., Veldink, J.H., van den Berg, L.H., van den Heuvel, M.P., 2013. Structural brain network imaging shows expanding disconnection of the motor system in amyotrophic lateral sclerosis. Hum. Brain Mapp. 00, 1–11. http://dx.doi.org/10.1002/hbm.22258.

Zhou, J., Gennatas, E.D., Kramer, J.H., Miller, B.L., Seeley, W.W., 2012. Predicting regional neurodegeneration from the healthy brain functional connectome. Neuron 73, 1216–1227. http://dx.doi.org/10.1016/j.neuron.2012.03.004.

Supplementary Material

Computational axonal disease spread – cortical parcellations

Additional simulations of axonal disease spread performed on parcellations of the human cortex consisting of 68 and 219 regions, respectively, show good correspondence with simulations based on the 83-sized human parcellation (Figure 3-A) and with simulated aggregation levels in the macaque (Figure 5-C). The decreasing trend in simulated aggregation levels with advancing stage was observed to be significant using both null-models for the 68-sized parcellation ($p = 0.05$, compared with random permutations of pTPD-43 regions across stages (null-model a), $p < 0.001$, compared with random seed regions (null-model b)) and for the 219-sized parcellation ($p = 0.01$ (null-model a), $p = 0.005$ (null-model b)).

Group threshold

To assess the robustness of our findings against the setting of the group threshold, 60%, analyses and simulations were repeated for average connectome maps obtained using a group threshold of 50% and 70%, requiring connections to be present in at least 50% or 70% of the subjects, respectively.

First, a significantly higher level of connectivity strength between pTDP-43 regions was observed as compared to connections linking the pTDP-43 regions to the rest of the brain (group threshold 50%: factor 1.11, *t*-test, $p = 1.2*10^{-5}$; group threshold 70%: factor 1.10, *t*-test, $p = 4.8*10^{-5}$) and the internal wiring strength of the pTDP-43 subnetwork was found to be significantly stronger than expected based on 1,000 random subnetworks (group threshold 50%: $p = 0.02$; group threshold 70%: $p = 0.03$). Second, a significant ordering of increasing network topological distances was present between

regions of more distant stages (i.e. I->I, I->II, I->III, I->IV, group threshold 50%: p = 0.002; group threshold 70%: p = 0.003, 1,000 random permutations of stage assignments). Third, *in silico* simulations resulted in aggregation levels decreasing with more advanced stages, overlapping the observed pTDP-43 staging (group threshold 50%: p = 0.016 compared with 1,000 random permutations of stage assignments to pTDP-43 regions (null-model a), p = 0.013 compared with random seed regions (null-model b); group threshold 70%: p = 0.015 (null-model a), p = 0.011 (null-model b)). In summary, the group threshold has little effect on our findings over a wide range of settings (50% - 70%).

Number of steps of random walker

The initial random walker in our connectome-based model of axonal disease spread was allowed to make 5 steps. Here, simulated aggregation levels across pTDP-43 stages were reevaluated while letting the initial random walker take 2, 4, 6, or 8 steps, Figure S2. For short walk lengths (2 and 4 steps) a large contrast in simulated aggregation levels was observed between stage I and the subsequent stages, which is a result of stage I regions being the *seed* regions and of the random walks being terminated after 2 or 4 steps, often not including any of the other pTDP-43 regions. Increasing the walk lengths, more regions of the pTDP-43 subnetwork will be visited, yielding a better reflection of how the topological organization of the pTDP-43 subnetwork may give rise to levels of pTDP-43 aggregation. However, for long random walks (8 or more steps), the entire brain network becomes involved and the simulated aggregation levels begin to reflect the nodal strengths (sum of all of a node's connection weights). With mean nodal strengths (SD) of stage I, II, III and IV regions as follows:

Stage I: 21.0 (8.7),

Stage II: 8.9 (6.7),

Stage III: 13.4 (4.8),

Stage IV: 8.3 (3.3),

the longer the walk length the more the simulated aggregation levels across stages reflect the ordering among mean nodal strengths of stages, with highest levels in stage I, followed by stage III, then stage II and lowest levels in stage IV (Figure S2, 8 steps). Hence, the number of steps of the initial walker was set to 5 in the main analysis (Figure 3), providing good coverage of all regions in the pTDP-43 subnetwork while random walks were short enough to prevent the aggregation levels to be a direct result of the nodal strengths.

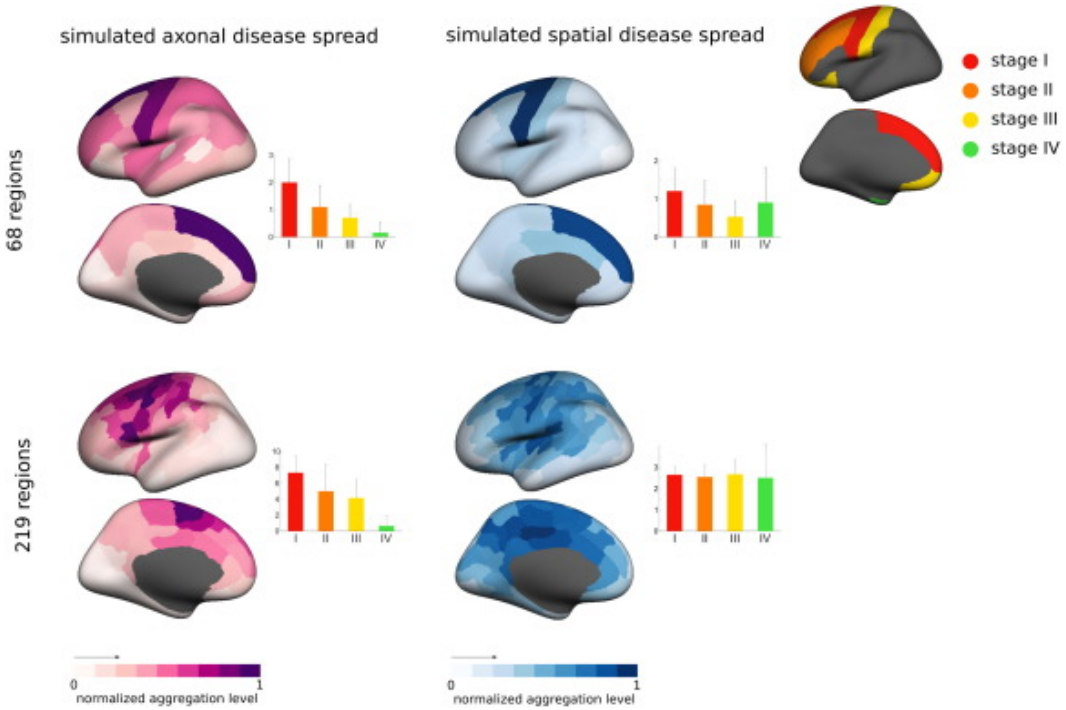

Fig. S1. Distribution of simulated aggregation levels, modeling axonal disease spread (left column) or spatial disease spread (right column), across the human cortex using a 68 and 219 sized parcellation scheme. Graphs show simulated aggregation levels evaluated per stage of neuropathology to overlap with the sequential stages of pTDP-43 neuropathology for the axonal model of disease spread. Simulated aggregation levels using the spatial model show no correspondence with neuropathological staging.

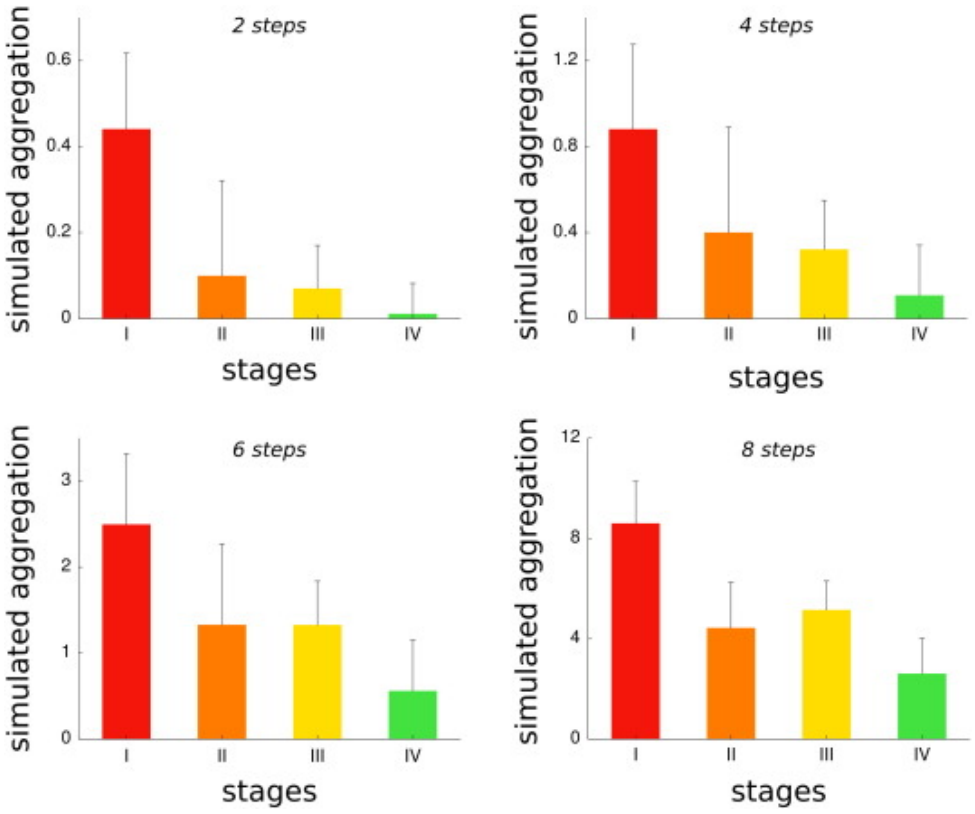

Fig. S2. Simulations of axonal spread on the basis of anatomical wiring of the healthy human connectome were rerun for different settings of random walker lengths (2, 4, 6, and 8 steps).

The trend of decreasing simulated aggregation levels with advancing stages, overlapping the empirical findings of Brettschneider, persists over walker lengths ranging from 2 to 6 steps. Using longer walk lengths yielded higher levels of aggregation in stage III than in stage II reflecting the higher mean nodal strength of stage III regions compared with stage II regions.

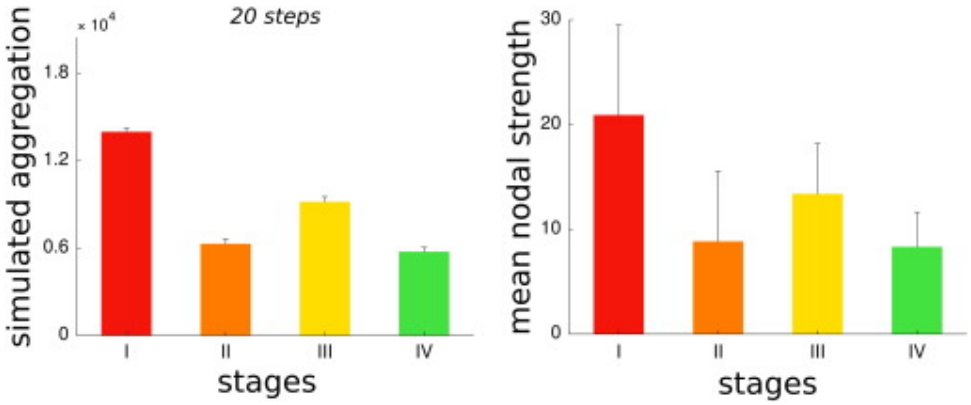
20 steps
× 10^4
simulated aggregation
1.8
1.2
0.6
0
I
II
III
IV
stages
mean nodal strength
30
20
10
0
I
II
III
IV
stages

Fig. S3.